Fuel Cladding post-quench LOCA Embrittlement: Mechanical test Relevance

Severine Guilbert, Jean Desquines

Fuel Cladding post-quench LOCA Embrittlement: Mechanical test Relevance

Séverine Guilbert-Banti[1], Jean Desquines[1]

[1]*Institut de Radioprotection et de Sûreté Nucléaire, PSN-RES/SEREX/LE2M, F-13115 Saint Paul lez Durance, France*
+33 4 42 19 95 56 and severine.guilbert@irsn.fr

Abstract. During a loss-of-coolant-accident (LOCA), the fuel cladding is submitted to a high temperature increase in a steam environment, along with an internal pressure increase which would eventually lead to ballooning and burst of the cladding. Steam could then penetrate through the burst opening and lead to inner surface oxidation and secondary-hydriding of the cladding. Post-quench cladding rupture can then occur either in two-sided oxidized area with wall thinning due to ballooning, or in single-sided oxidized area with large hydrogen content.

Common tests involved in the evaluation of the post-quench ductility are Ring Compression Tests (RCT) [1-4], Expansion Due to Compression Test (EDC) [5] or Axial Tensile Tests (AT) [6].

Questions arise about these mechanical tests, as for instance, the influence on sample failure of the oxide layer thickness partitioning between inner and outer diameter.

A systematic study was carried out to compare several mechanical tests on both single-sided and two-sided Zircaloy-4 oxidized samples. Five different mechanical tests were compared, including RCT: "C"-shaped ring Compression Test (CCT), Axial Tensile test (AT), Ring Tensile Test with well-defined machined gage section (RTT) and plain Ring Tensile Test (pRTT). All samples were taken from cladding tubes which had been oxidized in steam at 1200°C and then water-quenched. Mechanical tests were performed at room temperature and two to three samples were tested for each oxidation conditions and for every sample geometry to assess the reproducibility. Metallographic examinations were carried out to measure the ZrO_2 and $\alpha Zr(O)$ layer thicknesses and the ex-$\beta/\alpha(O)$ phase fraction. Mean hydrogen content measurements were also performed systematically on each sample.
Results indicate that the different mechanical tests have not the same sensitivity to the oxide layer partitioning: RTT and pRTT load at failure seems to depend mainly on the cumulated oxide layer thickness rather than on its partitioning, whereas this parameter has an impact on CCT and AT test results. For all tensile tests, stresses at failure were derived from load-displacement curves. The failure of brittle samples was assumed to be governed by linear elastic fracture mechanics. Using conventional stress intensity factor solution, a value of the material fracture toughness controlling the sample failure was determined from experimental results and discussed.

Keywords: Zircaloy, Mechanical Testing, LOCA.

INTRODUCTION

During a loss-of-coolant-accident (LOCA), the fuel cladding is submitted to a high temperature increase in a steam environment, along with an internal pressure increase which would eventually lead to ballooning and burst of the cladding. Steam could then penetrate through the burst opening and lead to inner surface oxidation and secondary-hydriding of the cladding. Post-quench cladding rupture can then occur either in two-sided oxidized area with wall thinning due to ballooning, or in single-sided oxidized area with large hydrogen content.

Several mechanical tests are usually used to evaluate the degree of material embrittlement after a LOCA transient: tests controlled by bending such as Ring Compression Tests (RCT) [1-4], or tests controlled by rather homogeneous tensile stress components such as Expansion Due to Compression Test (EDC) [5], Axial Tensile Tests

(AT) [6] or Hoop Tensile Tests. Comparable tests are involved in the determination of cladding fracture toughness in the axial direction [7]. Each mechanical test has its advantages and disadvantages.

Hoop Tensile Tests with well-defined gage section (RTT) rely on sample stretching using two mandrels. The mandrels are usually machined by cutting a cylindrical bar into two halves; some additional thickness is then removed over the flat surface in order to facilitate mandrel insertion into the sample. If the mandrel diameter is smaller than the inner diameter of the cladding tube, then the test starts with a bending phase until the entire mandrel surfaces are in contact with the inner cladding surface. If the mandrel diameter is higher than the sample inner diameter, frictional forces also develop. The bending phase can be reduced by inserting an additional part, called "dog-bone", between the mandrels [8, 9]. However, the insertion of this additional part introduces frictional forces due to the direct contact between the dog-bone and the specimen. Hoop Tensile Test can also be performed on plain ring without well-defined gage section (pRTT) [10, 11]. The RTT and pRTT tests cannot be fully considered as hoop tensile tests, a rather short region is actually loaded in this direction. Additionally, the hoop extension of the gage section strongly depends on friction coefficient between the mandrels and the inner side of the samples. The sample behavior is known to be influenced by lubrication under close testing conditions for these two tests [7, 8]. Expansion Due to Compression Test consists in compressing axially a soft pellet inserted in the cladding tube. The ends of the sample are free to move axially, therefore, limited axial compression stress is generated in the cladding [12]. The hoop stress field during an EDC test is quite homogeneous azimuthally [13]. However, several friction effects can influence the test (piston/pellet, pellet/cladding, piston/cladding) and the test temperature is limited to a maximum temperature due to the soft pellet material properties (Teflon, aluminum or copper). Axial Tensile Test consists in applying a tensile load to double-leg samples [14]. This test is governed by rather uniform axial stress determined straightforward as the ratio between applied load and gage cross section. Integral Thermal Shock tests are also used for fuel cladding studies and rely on load-controlled conditions [15, 16]. This type of test is closer to LOCA conditions but also higher complexity to analyze the phenomena. Ring Compression Test is based on transverse compression of a ring of cladding tube [1, 17]. This test is a good ductility screening test to study the ductile/brittle transition. However, it leads to inhomogeneous stress distribution rather governed by a complex bending hoop component varying azimuthally. An alternative to RCT can be "C"-shaped ring Compression Test (CCT) [18]. For CCT, the loading is almost pure bending in the hoop direction inducing a maximum stress value at outer diameter and equatorial location.

To get a clearer view on these different mechanical tests and their response regarding the oxide layer partitioning, a study has been launched and results are presented in this paper. EDC test was not considered due to its complexity induced by the association of several materials properties and large strains and displacements but also intense friction. During EDC tests, the strains can be measured but the stress distribution cannot be accurately deduced. Single or two-sided oxidation of Zircaloy-4 cladding tubes was performed under steam at 1200°C. Oxidation was interrupted by water-quench. Then, five different mechanical tests were compared, including RCT: "C"-shaped ring Compression Test (CCT), Axial Tensile test (AT), Hoop Tensile test with well-defined machined gage section (RTT) and Hoop Tensile test on plain rings (pRTT). Mechanical tests were performed at room temperature and two to three samples were tested for each oxidation conditions and for every mechanical test to compare the testing techniques and to assess the reproducibility. Metallographic examinations were carried out to measure the ZrO_2 and αZr(O) layer thicknesses and the ex-β/α(O) phase fraction. Hydrogen contents were measured.

MATERIAL AND METHODS

Samples preparation

The specimens used in this study were cut from Zircaloy-4 AFA2G stress relieved annealed (SRA) industrial cladding tubes, provided by AREVA-NP. The alloy composition is given in TABLE 1. The outer diameter and wall thickness of the tubes are 9.5 mm and 570 µm respectively.

TABLE 1. Chemical composition of the Zy-4 batch used in this study.

Sn (wt%)	Fe (wt%)	Cr (wt%)	O (wt%)	H (wppm)
1.30	0.21	0.10	0.12	10

Testing protocol

Specimen geometry and configurations

Five different mechanical tests were systematically carried out for each experimental condition:

- Ring Compression Test (RCT): Tests were performed on 10 mm long specimens.
- C-shaped ring Compression Test (CCT). Tests were performed on 10 mm long specimens.
- Axial Tensile test (AT): Tests were performed on 70 mm long specimens (FIGURE 1 (a)).
- Machined Hoop Tensile Test (RTT): Tests were performed on 5 mm long specimens (FIGURE 1 (b)).
- Hoop Tensile Test (pRTT): it requires 5 mm long ring specimen.

No lubrication was used for any of the above mentioned tests. A slight difference in friction coefficient is expected depending on the oxidation state of the contact surfaces (for example contact between mandrel and inner surface of pRTT and RTT).

Cutting/Machining

The first step of the protocol consisted in cutting and machining the samples.

For one-sided oxidation tests, Zircaloy-4 caps were welded on 70 mm long samples using electron beam. Ring cutting, and milling of the AT and RTT samples was performed after high temperature (HT) oxidation.

For two-sided oxidation tests, the AT samples were spark machined before oxidation. For CCT, RCT, RTT and pRTT, 30 to 40 mm long samples were cut using a diamond saw prior to oxidation. After oxidation, 5 or 10 mm long rings were cut using again the diamond saw. Milling of the RTT was performed after HT oxidation in a 5 mm long ring.

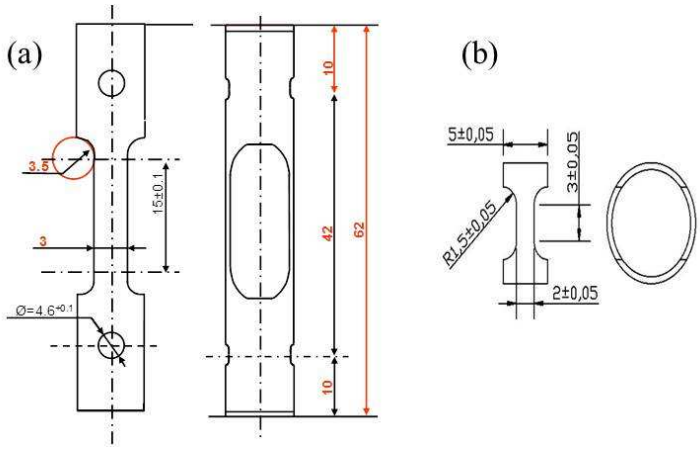

FIGURE 1. AT (a) and RTT (b) specimen geometries. Dimensions are expressed in millimeters.

Oxidation

Samples were oxidised in a vertical resistive furnace in a steam + argon flow at 1200°C. The argon and steam flow rates were respectively 10 $Nl.min^{-1}$ and 500 $g.h^{-1}$ (50% vol. Ar and 50% vol. steam). After the high temperature oxidation, the sample was water-quenched by dropping into a water bath.

Mechanical testing

All the mechanical tests were performed at room temperature using an INSTRON 5566 electromechanical test device. Load-displacement was recorded for each mechanical test.

The tests were carried out with a constant displacement rate of 0.016 mm/s. The CCT and RCT test consists in compressing the sample up to sample failure. A 1 kN load cell was used for these tests (measurement uncertainty 0.25% with a 95% confidence level). For RTT and pRTT, two half cylindrical mandrels were used to apply a transverse tensile load to the sample. Five pairs of mandrels made of 718 Inconel were available. Their diameter range from 8.20 to 8.36 mm, to adjust diameter to the sample inner diameter. For AT, loading was applied up to sample failure and tests were video-recorded in order to determine which of the two-legs failed first (when possible).

Either a 5 kN or a 10 kN load cell was used for the tensile tests (measurement uncertainty 0.25% with a 95% confidence level).

Sample characterization

Weight and length of the samples were measured before and after oxidation with an accuracy of 0.1 mg and 0.01 mm respectively. Sample weight before and after oxidation was used to determine the weight gain, giving a direct measurement of the Equivalent Cladding Reacted (ECR).

After the HT steam oxidation, metallographic cut were taken for every sample. For AT samples, the leg corresponding to the first rupture was taken for metallography. On each metallographic cut, the thicknesses of the oxide and α-Zr(O) layers were measured at eight different locations at both outer and inner surfaces. Mean thickness values were calculated as the average of 32 measurements. Metallographs were also used for image analysis to determine the αZr(O)/β phase fraction.

Global hydrogen content was measured by the hot extraction technique using a Brücker ONH mat 286. Mean hydrogen concentrations were calculated as the average of 6 measurements for every steam oxidized sample. When possible, the mean hydrogen concentrations were also measured on as-received samples (on scraps resulting from machining of the axial tensile sample legs).

Test matrix

The test program includes 72 samples, with measured ECR ranging from 10 to 27%, either for one or two-sided oxidation (TABLE 2).

TABLE 2. Test matrix, including oxidation duration, Baker-Just (BJ) [19] and measured ECR, the number of samples for each mechanical test and testing condition.

Oxidation duration (s)	One (OS) or two-sided (TS) oxidation	ECR BJ (%)	Measured ECR (%)	Mechanical tests/number of tested samples				
				RCT	CCT	AT	RTT	pRTT
116	TS	14	10	4	5	3	3	4
236	TS	21	17			2		
465	TS	29	21	2	3	3	5	3
500	TS	31	24			1		
560	TS	32	25			1		
465	OS	11	10	3	3	1	2	3
1120	OS	17	17			1		
1200	OS	18	18			1		
1280	OS	18	18.5			1		
1365	OS	18.5	19			2		
1860	OS	22	22	3	3	2	3	3
2700	OS	27	27			2		

EXPERIMENTAL RESULTS

Oxidation results

After steam oxidation, metallographs show the presence of a dense and uniform oxide layer and an αZr(O) layer underneath, either on both inner and outer side for two-sided oxidation or on outer side for one-sided oxidation. The absence of inner side oxide layer for one-sided oxidation confirms the tightness of the welded caps. Beneath the αZr(O) layer, prior-β phase is observed. The prior-β phase is mixed with αZr(O) inclusions for measured ECR of 17% or higher. The typical microstructure of Zircaloy-4 samples after steam oxidation at 1200°C is illustrated in FIGURE 2.

The measured values of ZrO_2 and αZr(O) layer thicknesses are plotted in FIGURE 3 versus steam oxidation duration. The correlation of Cathcart-Pawel [20] for ZrO_2 and αZr(O) thicknesses are also plotted in FIGURE 3. The zirconia

layer measured thickness is in good agreement with the Cathcart-Pawel correlation, whereas the Cathcart-Pawel correlation rather underestimates the αZr(O) thickness.
The analyses of metallographies reveal the presence of radially-axially oriented cracks in the αZr(O) layer. These cracks never propagate in the zirconia layer, except for the one leading to sample failure.

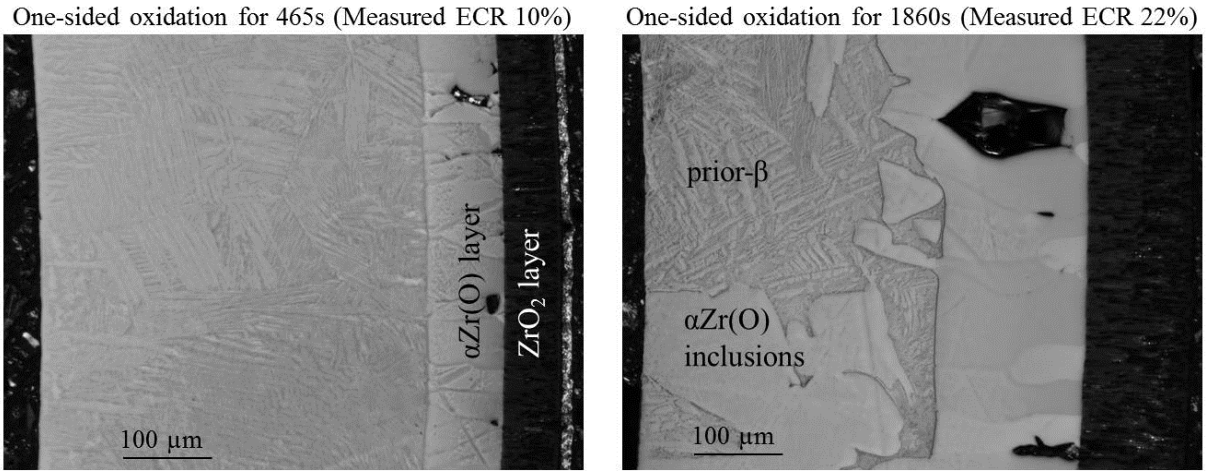

FIGURE 2. Optical micrographs of Zircaloy-4 after steam oxidation at 1200°C.

In order to determine the α-phase fraction from the metallography after the mechanical testing, the metallography is transformed into a binary image in the metallic part to distinguish the α-phase from the prior β-phase. This image is then used to determine the volume fraction of α-phase in the metallic part. The α-phase fraction is plotted in FIGURE 4 versus the measured ECR. The α-phase fraction is well correlated to the ECR and the influence of hydrogen on the phase fraction seems negligible.
The sample hydrogen content was measured before and after steam oxidation. The hydrogen pickup is 20 wppm at most.

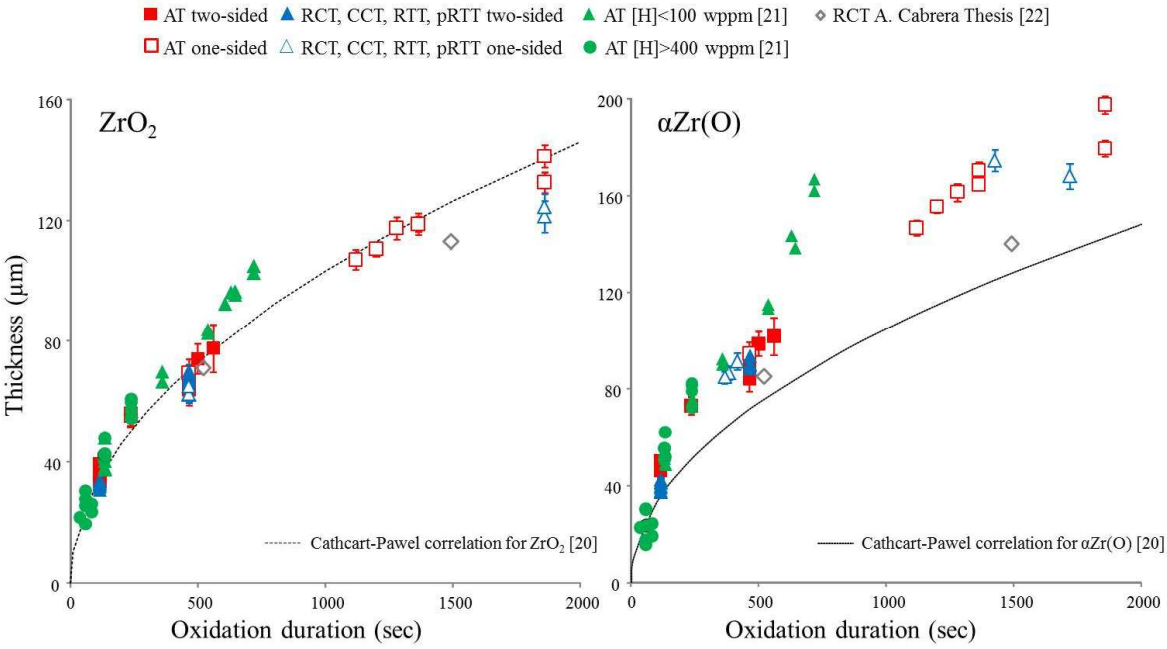

FIGURE 3. ZrO_2 and αZr(O) layer thicknesses after steam oxidation at 1200°C. Comparison with previous data from [21] and from [22].

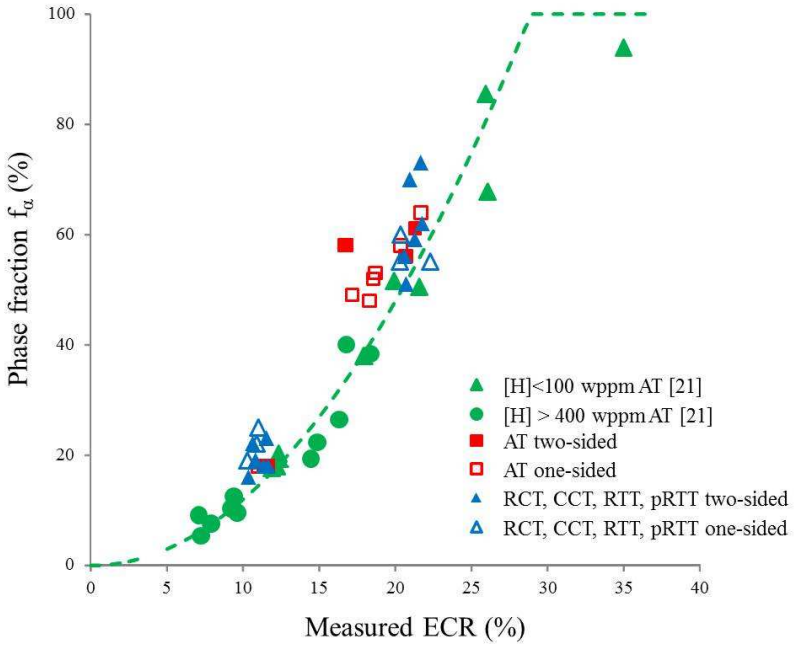

FIGURE 4. α-phase fraction in Zircaloy-4 after steam oxidation at 1200°C. Comparison with previous results [21].

Mechanical testing

Tensile tests

Tensile tests were performed in the cladding axial and hoop directions. The fracture loads for hoop tensile tests and axial tensile tests are respectively represented on FIGURE 5 (a) and (b). For RTT and pRTT, no significant difference in the tensile fracture load is observed between one-side and two-side oxidized samples: the fracture load seems not to be sensitive on the oxide layer partitioning (inner or outer side). However, the fracture load depends on the global measured ECR. For ATT, the axial fracture loads depend on the global measured ECR. Furthermore, for high ECR (above 15 %), it seems that fracture loads are lower for one-side oxidized samples compared to two-side oxidized samples.

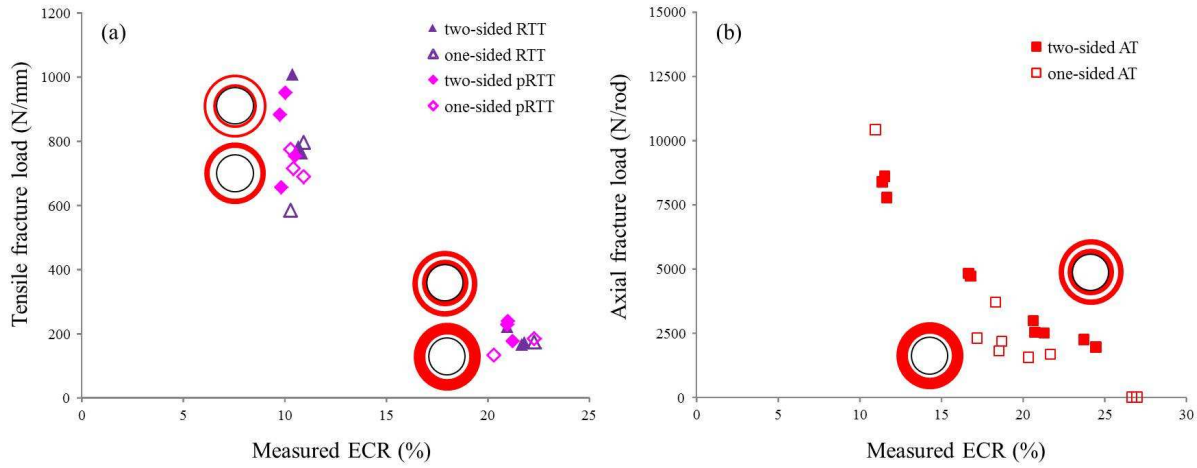

FIGURE 5. Fracture load for RTT, pRTT and ATT after steam oxidation at 1200°C.

Bending dominated tests

The fracture loads for ring and "C" shaped ring samples are represented on FIGURE 6 (a) and (b).

For RCT (FIGURE 6 (a)), the fracture load seems to be a function of the global measured ECR and not sensitive to the oxide layer location (inner or outer), as the same fracture loads were obtained for one-sided and two-sided specimens for a given ECR. However, it should be pointed out that, failure occurs at the equatorial location for one-sided samples and at the pole location for two-sided samples. So, RCT results are rather complex to interpret and require finite element analysis. For CCT, the stress is heterogeneous and its maximum value is obtained at outer diameter and equatorial location. FIGURE 6 (b) shows that for a given ECR, the fracture load is lower for one-side oxidized samples compared to two-side oxidized samples: this result is consistent since the outer oxide layer is thicker for one-sided oxidized sample than for two-sided one.

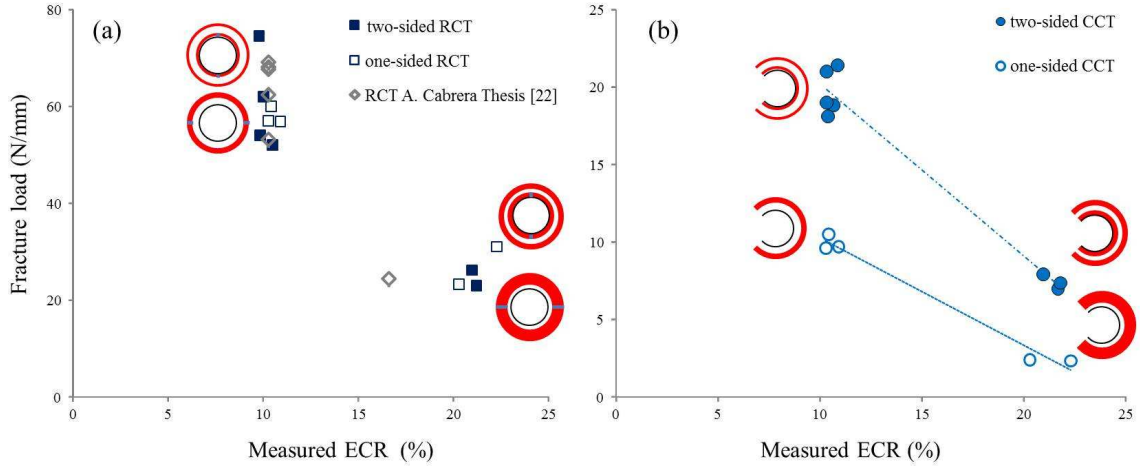

FIGURE 6. Fracture load for RCT and CCT after steam oxidation at 1200°C. Comparison with CEA results [22].

DISCUSSION

To compare the different tensile tests with each other, the failure stress was evaluated from the fracture load, in axial or hoop direction. FIGURE 7 represents the fracture stress versus the measured ECR for the ATT, RTT and pRTT after steam oxidation at 1200°C. The first important outcome of this comparison is that, the fracture stress is not significantly different between a mechanical test performed in the axial and hoop direction with or without a machined gage section.

Considering post-quench LOCA embrittlement, the sample is strongly embrittled and the stress intensity factor is expected to be a relevant material property. More, specifically, when the plastic zone at the crack tip has a negligible size compared to the crack depth, this situation is considered to be achieved for fracture toughness values below about 12 MPa√m. The sample failure is expected to happen when the stress intensity factor (K_I) is equal to the material fracture toughness (K_{Ic}) [21]. The material fracture toughness was evaluated using the failure stress of brittle samples and the formula of the Tada and Paris handbook (1, 2, 3) [23]:

$$K_{Ic} = \sigma \times F\left(\frac{a}{e}\right) \times \sqrt{\pi \times a} \tag{1}$$

where a is the crack depth, and e is the cladding thickness.

For a two-sided oxidation, leading to two symmetrical cracks with depth a:

$$F\left({}^{a}/_{e/2}\right) = \frac{1{,}122 - 0{,}561 \times \frac{a}{e/2} - 0{,}205 \times \left(\frac{a}{e/2}\right)^2 \mp 0{,}471 \times \left(\frac{a}{e/2}\right)^3 - 0{,}190 \times \left(\frac{a}{e/2}\right)^4}{\sqrt{\left(1 - \frac{a}{e/2}\right)}} \tag{2}$$

For a one-sided oxidation, leading to a lateral crack with depth a:

$$F({}^{a}/_{e}) = \frac{\sqrt{{}^{e}/_{\pi \times a}} \times \sqrt{2 \times \tan\left(\pi \times {}^{a}/_{2e}\right)} \times \left(0{,}752 + 2{,}02 \times \frac{a}{e} + 0{,}37 \times \left(1 - \sin\left(\pi \times \frac{a}{2e}\right)\right)\right)^3}{\cos\left(\pi \times {}^{a}/_{2e}\right)} \tag{3}$$

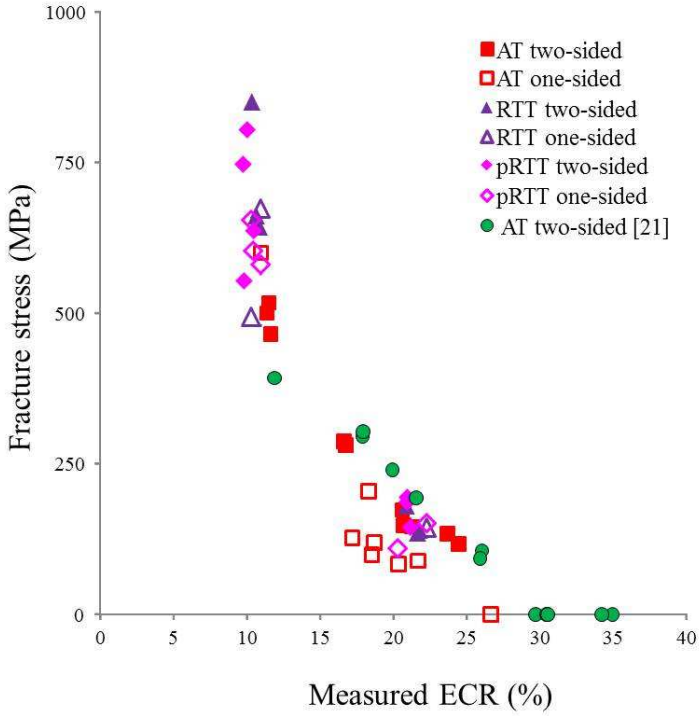

FIGURE 7. Fracture stress versus measured ECR after steam oxidation at 1200°C. Comparison with previous results [21].

The crack tip, before crack instability, being located in the prior-β phase, crack depth is estimated as the sum of the ZrO_2 and αZr(O) layer thicknesses, $a = e_{ZrO_2} + e_{\alpha(O)}$ and the fracture toughness is plotted versus the hydrogen content in the prior-β phase in FIGURE 8. The hydrogen content in the prior-β phase was estimated from the global hydrogen content measured by hot extraction and from the α-phase fraction, assuming that all hydrogen diffuses in the β-phase during the steam oxidation [2].

Thus, the fracture toughness seems well-correlated to the hydrogen content in the prior-β phase, not depending on the oxidation conditions (one or two-sided). A strong decrease of the fracture toughness is observed for hydrogen contents in the prior-β phase between 10 and 100 wppm. For larger hydrogen contents in the prior-β phase, the fracture toughness slightly decreases with hydrogen increasing content. The obtained values for fracture toughness are quite close to usual values obtained for ceramics.

The same approach was applied for CCT using the shape function correlation from [24]. As for tensile tests, the crack depth is estimated as the sum of the ZrO_2 and αZr(O) layer thicknesses. The values of fracture toughness for these tests, plotted in FIGURE 8, are consistent with the ones obtained from tensile tests.

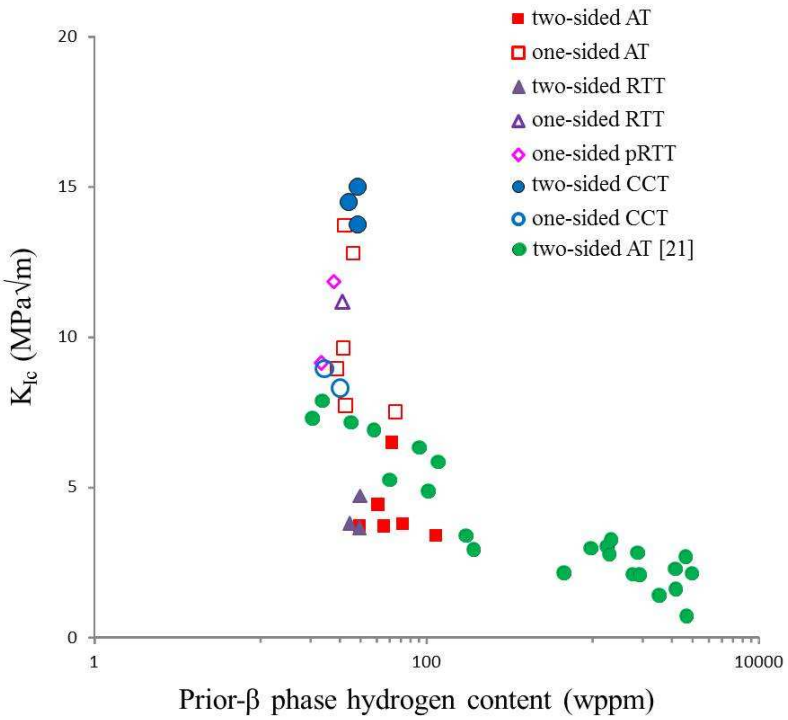

FIGURE 8. Fracture toughness versus hydrogen content in the prior-β phase. Comparison with previous results [21].

CONCLUSION

Five different mechanical tests (RCT, CCT, AT, RTT, pRTT) were compared on both single-sided and two-sided Zircaloy-4 oxidized samples. The objective was to get a better understanding of their response regarding the oxide layer partitioning.

Results indicate that the different mechanical tests have not the same sensitivity to the oxide layer partitioning: RTT and pRTT loads at failure seem to depend rather on the cumulated oxide layer thickness than on its partitioning, whereas this parameter has an impact on CCT and AT test results. RCT fracture loads seem to be a function of the global measured ECR and apparently not sensitive to the oxide layer location. This conclusion is surprising and careful use is recommended.

Regarding the tensile tests, the first important outcome of this comparison is that, the fracture stress is not significantly different between a mechanical test performed in the axial and hoop direction with or without a machined gage section. Comparing RTT and pRTT, authors consider that there is no need to machine a gage section and pRTT is sufficient when the samples are brittle.

Assuming that the failure of brittle samples was controlled by linear elastic fracture mechanics, a value of the material fracture toughness controlling the sample failure was determined from experimental results. Results show that the fracture toughness seems well-correlated to the hydrogen content in the prior-β phase.

ACKNOWLEDGMENTS

Authors are grateful to P. Lacote and G. Taraud for their technical assistance, for performing the oxidation tests, for metallography and EPMA. Authors would like to thank also EDF for its financial support.

REFERENCES

[1] Billone, M., Y. Yan, T. Burtseva and R. Daum, Cladding Embrittlement During Postulated Loss-of-Coolant Accidents, US-NRC, NUREG-CR-6967, (2008).

[2] Brachet, J.C., V. Vandenberghe-Maillot, L. Portier, D. Gilbon, A. Lesbros, N. Waeckel and J.-P. Mardon, Hydrogen Content, Preoxidation, and Cooling Scenario Effects on Post-Quench Microstructure and Mechanical Properties of Zircaloy-4 and M5 Alloys in LOCA conditions, *in Zirconium in Nuclear Industry: 15th International Symposium, ASTM STP 1505*, (2008), Sunriver, Oregon, ASTM International.

[3] Vrtilkova, V., Review of Recent work at UJP PRAHA on the LOCA Embrittlement Criterion, *in 6th Plenary Meeting of the OECD/CSNI/SEGFSM*, (2005), Paris.

[4] Udagawa, Y., F. Nagase and T. Fuketa, Effect of Cooling History on Cladding Ductility under LOCA Conditions, *Journal of Nuclear Science and Technology*, (2006), **43**(8), p. 844-850.

[5] Le Saux, M., J. Besson, S. Carassou, C. Poussard and X. Averty, Behavior and failure of uniformly hydrided Zircaloy-4 fuel claddings between 25 °C and 480 °C under various stress states, including RIA loading conditions, *Engineering Failure Analysis*, (2010), **17**(3**)**, p. 683-700.

[6] Portier, L., T. Bredel, J.C. Brachet, V. Maillot, J.P. Mardon and A. Lesbros, Influence of Long Service Exposures on the Thermal-mechanical Behavior of Zy-4 and M5 Alloys in LOCA conditions, *in Zirconium in the Nuclear Industry: 14th International Symposium, ASTM STP 1467*, (2004), Stockholm, Sweden, ASTM International, West Conshohocken, PA.

[7] Yagnik, S., N. Ramasubramanian, V. Grigoriev, C. Sainte-Catherine, J. Bertsch, R. Adamson, R.-C. Kuo, S.T. Mahmood, T. Fukuda, P. Efsing, and B.C. Oberländer, Round-Robin Testing of Fracture Toughness Characteristics of Thin-Walled Tubing, *in Zirconium in the Nuclear Industry, 15th International Symposium*, (2008), Sunriver, Oregon, USA, Journal of ASTM International.

[8] Arsène, S. and J. Bai, A New Approach to Measuring Transverse Properties of Structural Tubing by a Ring Test - Experimental Investigation, *Journal of Testing and Evaluation*, (1998), **26**(1), p. 26-30.

[9] Arsène, S., Effet de la microstructure et de la température sur la transition ductile-fragile des Zircaloy hydrurés, PhD Thesis, Ecole Centrale de Paris, France (1997).

[10] Hong, S.I., K.W. Lee and K.T. Kim, Effect of the circumferential hydrides on the deformation and fracture of Zircaloy cladding tubes, *Journal of Nuclear Materials*, (2002), **303**(2–3), p. 169-176.

[11] Racine, A., Influence de l'orientation des hydrures sur les modes de déformation, d'endommagement et de rupture du Zircaloy-4 hydruré, PhD Thesis, Ecole Polytechnique, France (2005).

[12] Hellouin de Menibus, A., Q. Auzoux, O. Dieye, V. Macdonald, J. Besson and J. Crépin, Hydride blisters Formation, Characterization and Effect on the Fracture of Zircaloy-4 Cladding Tubes Under Reactivity Initiated Accident, *in 21st International Conference Nuclear Energy for New Europe*, (2012), Ljubljana, Slovenia.

[13] He, M., Caractérisation du comportement à rupture des alliages de zirconium de la gaine du crayon combustible des centrales nucléaires dans la phase post-trempe d'un APRP (Accident de Perte de Réfrigérant Primaire), PhD Thesis, Ecole Nationale Supérieure des Mines de Paris, France (2012).

[14] Le Saux, M., J. Besson, S. Carassou, C. Poussard and X. Averty, A model to describe the anisotropic viscoplastic mechanical behavior of fresh and irradiated Zircaloy-4 fuel claddings under RIA loading conditions, *Journal of Nuclear Materials*, (2008), **378**(1), p. 60-69.

[15] Nagase, F., T. Chuto and T. Fuketa, Behavior of high Burn-up fuel Cladding Under LOCA Conditions, *Journal of Nuclear Science and Technology*, (2009), **46**(7), p. 763-769.

[16] Nagase, F. and T. Fuketa, Results from Studies on High Burn-up Fuel Behavior Under LOCA Conditions, *in Nuclear Safety Research Conference*, (2004), Washington, DC, USA.

[17] Kim, J.H., M.H. Lee, B.K. Choi and Y.H. Jeong, Embrittlement Behavior of Zircaloy-4 Cladding During Oxidation and Water Quench, *Nuclear Engineering and Design*, (2005), **235**, p. 67-75.

[18] Desquines, J., D. Drouan, P. March, S. Fourgeaud, C. Getrey, V. Elbaz and M. Philippe, Characterization of Radial Hydride Precipitation in Zy-4 using "C"-shaped samples, *in LWR Fuel Performance Meeting TopFuel 2013*, Charlotte, NC

[19] Baker, L. and L.C. Just, Studies of Metal-Water Reactions at high Temperatures. III Experimental and Theoretical Studies of the Zirconium-Water Reaction, Argonne National Laboratory, ANL-6548, (1962).

[20] Cathcart, J.V., R.E. Pawel, R.A. McKee, R.E. Druschel, G.J. Yurek, J.J. Campbell and S.H. Jury, Zirconium Metal-Water Oxidation Kinetics IV. Reaction rate Studies, ORNL/NUREG-17, (1977).

[21] Desquines, J., D. Drouan, S. Guilbert and P. Lacote, Embrittlement of pre-hydrided Zircaloy-4 by steam oxidation under simulated LOCA transients, *Journal of Nuclear Materials*, (2016), **469**, p. 20-31.

[22] Cabrera-Salcedo, A., Modélisation du comportement mécanique "post-trempe", après oxydation à haute température, des gaines de combustible de réacteurs à eau pressurisée, PhD Thesis, Mines ParisTech, France (2012).

[23] Tada, H., P.C. Paris and G.R. Irwin, The Stress Analysis of Cracks Handbook, ed. P. Production (1985), Saint Louis, USA.

[24] Desquines, J., D. Drouan, E. Torres, S. Guilbert and P. Lacote, An attempt for a unified description of mechanical testing on Zircaloy-4 cladding subjected to simulated LOCA transient, *in LWR Fuel Performance Meeting Topfuel*, (2015), Zurich, Switzerland.